Thin Solid Films 518 (2010) 6839–6843

Contents lists available at ScienceDirect

Thin Solid Films

journal homepage: www.elsevier.com/locate/tsf

Aerosol assisted fabrication of metallic film/carbon fiber and heat treatment to form crystalline alloy film

Jeong Hoon Byeon [a], Ki Young Yoon [b], Jungho Hwang [b,c,*]

[a] LCD Division, Samsung Electronics Co., Ltd., Yongin 446-711, Republic of Korea
[b] School of Mechanical Engineering, Yonsei University, Seoul 120-749, Republic of Korea
[c] Yonsei Center for Clean Technology, Yonsei University, Seoul 120-749, Republic of Korea

ARTICLE INFO

Article history:
Received 22 October 2009
Received in revised form 15 June 2010
Accepted 30 June 2010
Available online 8 July 2010

Keywords:
Carbon fiber
Catalytic activation
Pd aerosol nanoparticles
Electroless films
Sintering

ABSTRACT

Carbon fiber (CF) was catalytically activated with spark generated Pd aerosol nanoparticles. Metal (Ag, Au, Cu, and Pd) and alloy (Ni–P, Ni–Cu–P) electroless films were deposited on Pd aerosol activated CF using a range of deposition parameters including deposition rate in an electroless deposition bath. Sintering was applied to the alloy films on the CF to examine the crystallization behavior at 400 °C in a nitrogen atmosphere. Ni–Cu–P had a higher crystallinity than Ni–P after the treatment.

1. Introduction

Metal/carbon fiber (CF) composites have been used in a variety of applications, such as environmental catalysts [1], reinforced materials [2], antimicrobial agents [3,4], electromagnetic interference shielding materials [5,6], radar absorbing materials [7], catalytic graphitizations [8], and composite membranes [9]. The techniques currently used for depositing metal films on fibrous substrates are conducting paints and lacquers, sputter coating, vacuum deposition, flame and arc spraying, and electroless deposition (ELD) [10]. Among them, ELD has advantages, such as coherent metal deposition, excellent conductivity, and applicability to complex-shaped materials or nonconductors. A range of metals, including Ag, Cu, Au, Co, Ni, and some alloys of these metals, can be deposited from an ELD bath [11,12].

The initiation of the ELD process is preceded by surface activation methods to provide catalytic sites (usually Pd) on the material surface [13–15]. Pd nanoparticles act as initiators of the subsequent ELD process. However, conventional Sn–Pd based activations require a long process time, intermittent water rinsing and drying, involve the loss of expensive metal ions, and create environmental pollution problems [16]. Since it is difficult to realize pure catalytic sites with a wet chemical activation method due to impurities inevitably involved, an aerosol activation using spark generated Pd nanoparticles [17] can be used to form catalytic sites on CF surface. This aerosol assisted process was used to effectively form Ag films on CF in a previous study [18].

Also co-deposition of particulate films or substances within the growing layer has led to a generation of electroless composite films [19]. In particular, Ni–P and Ni–Cu–P alloys are used extensively in industry due to their excellent wear and corrosion resistance and some special physical performances, e.g. magnetic properties, solderability, and polishability [20,21]. Applying sintering to alloy films produced significant increases in crystallinity and hardness, which contributed to increased electrical conductivity [22] and mechanical strength [20,23]. The crystallization behavior of the as-deposited alloy film and related properties at high or elevated temperatures has become increasingly important in applications of the materials [24]. However, it seems difficult to form crystalline alloy films on CF from amorphous alloy films just by heat treatment because of CF cracking and/or its property change with high temperature over 500 °C [25,26]. Thus, by applying a film property control on the CF it should be possible to avoid unwanted reaction at the interface between CF and alloy film and improve the crystallinity of the alloy film.

In our present work, Pd aerosol activation on CF was extensively used for various metals (Ag, Au, Cu, and Pd) and alloy (Ni–P and Ni–Cu–P) electroless films. The alloy films were achieved by co-deposition of the corresponding elements (Ni, P, and Cu) in an ELD bath. Sintering at high temperature (400 °C) in a nitrogen atmosphere, which reduces the risk of cracks of CF or unwanted interface reaction between CF and alloy film was carried out after co-deposition to investigate the crystallization behavior of the as-deposited alloy films.

* Corresponding author. Yonsei Center for Clean Technology, Yonsei University, Seoul 120-749, Republic of Korea. Tel.: +82 2 2123 2821; fax: +82 2 312 2821.
E-mail address: hwangjh@yonsei.ac.kr (J. Hwang).

0040-6090/$ – see front matter
doi:10.1016/j.tsf.2010.06.067

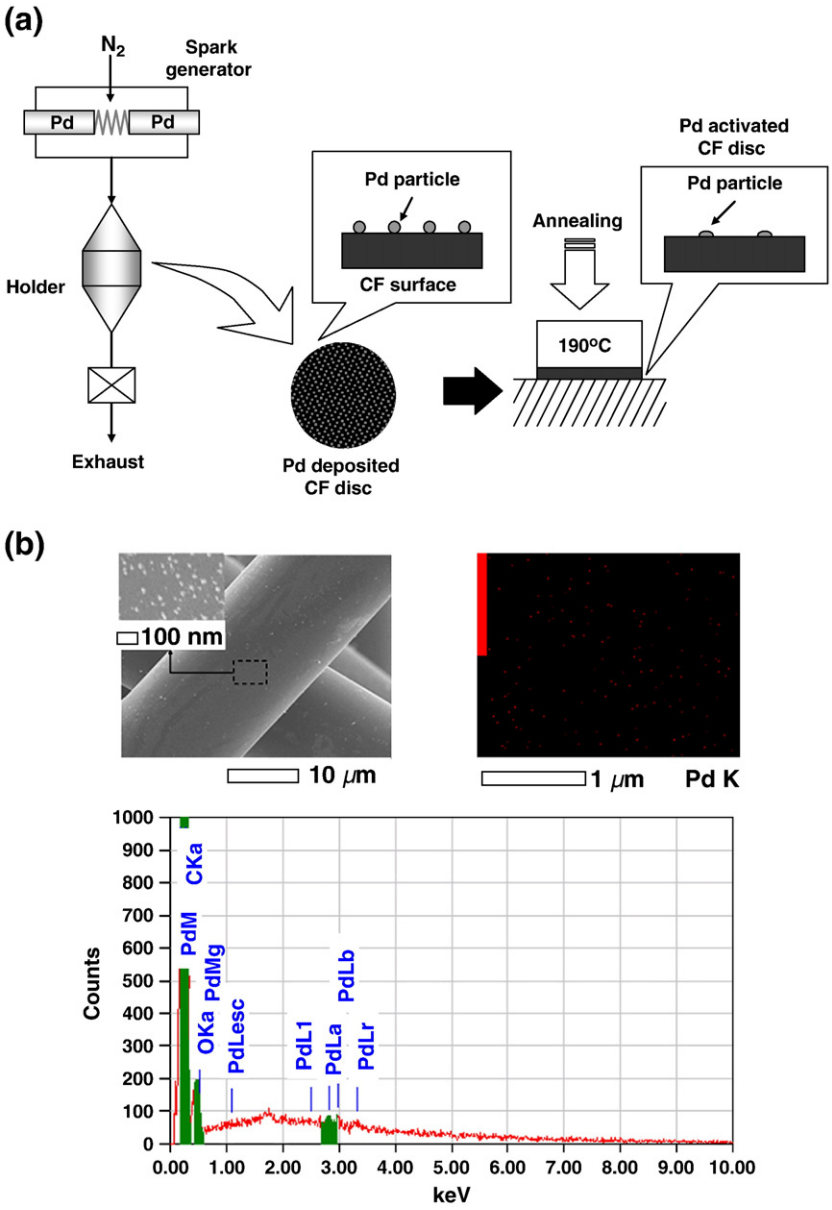

Fig. 1. (a) Schematic of aerosol activation procedure containing spark generation of Pd, collection of Pd nanoparticles on CF, and annealing of collected Pd on CF. (b) SEM micrographs and EDX results of the aerosol activated CF.

2. Materials and methods

The catalytic activation process (Fig. 1a) involved the spark generation of Pd aerosol nanoparticles and their filtration through a rayon-based porous CF (38 mm in diameter and 2.6 mm in thickness, KF-1600, Toyobo, Japan). The average length of CF and their mean separation distance were 9.1 mm and 22.4 μm, respectively. The activation involved fewer steps than conventional surface activation

Table 1
Compositions of the ELD baths and bath conditions.

ELD	Bath composition	Bath temperature (°C)
Ag	Solution A: 2 g/L $AgNO_3$, 60 g/L Na_2-EDTA·$2H_2O$, 88 mL/L isopropyl alcohol, 12 mL/L acetic acid, 400 mL/L NH_4OH Solution B: 3 mL/L hydrazine, 2 mL/L mercerine, 400 mL/L ethanol Mixture solutions of A and B at 1:1 (v/v)	30
Au	5 g/L $KAu(CN)_2$, 8 g/L KCN, 20 g/L NaOH, 10 g/L glycine, 25 g/L $NaBH_4$	90
Cu	Solution A: 30 g/L $CuSO_4$, 140 g/L sodium potassium tartrate, 40 g/L NaOH Solution B: aqueous formaldehyde solution (37.2 wt.%) Mixture solutions of A and B at 10:1 (v/v)	40
Pd	1.5 g/L $PdCl_2$, 40.1 g/L Na_2-EDTA·$2H_2O$, 195 mL/L NH_3·H2O (28%), 5 mL/L N_2H_4 (1 M)	50
Ni–P	15 g/L $NiSO_4$·$6H_2O$, 18 g/L $H_3C_6H_5O_7$·$6H_2O$, 30 g/L NaH_2PO_2·H_2O, 28 g/L $NaCH_3COO$·$3H_2O$, 20 mL/L lactic acid (85%), 2 mg/L thiourea	75
Ni–Cu–P	12 g/L $NiSO_4$·$6H_2O$, 3 g/L $CuSO_4$·$6H_2O$, 18 g/L $H_3C_6H_5O_7$·$6H_2O$, 30 g/L NaH_2PO_2·H_2O, 28 g/L $NaCH_3COO$·$3H_2O$, 20 mL/L lactic acid (85%), 2 mg/L thiourea	60

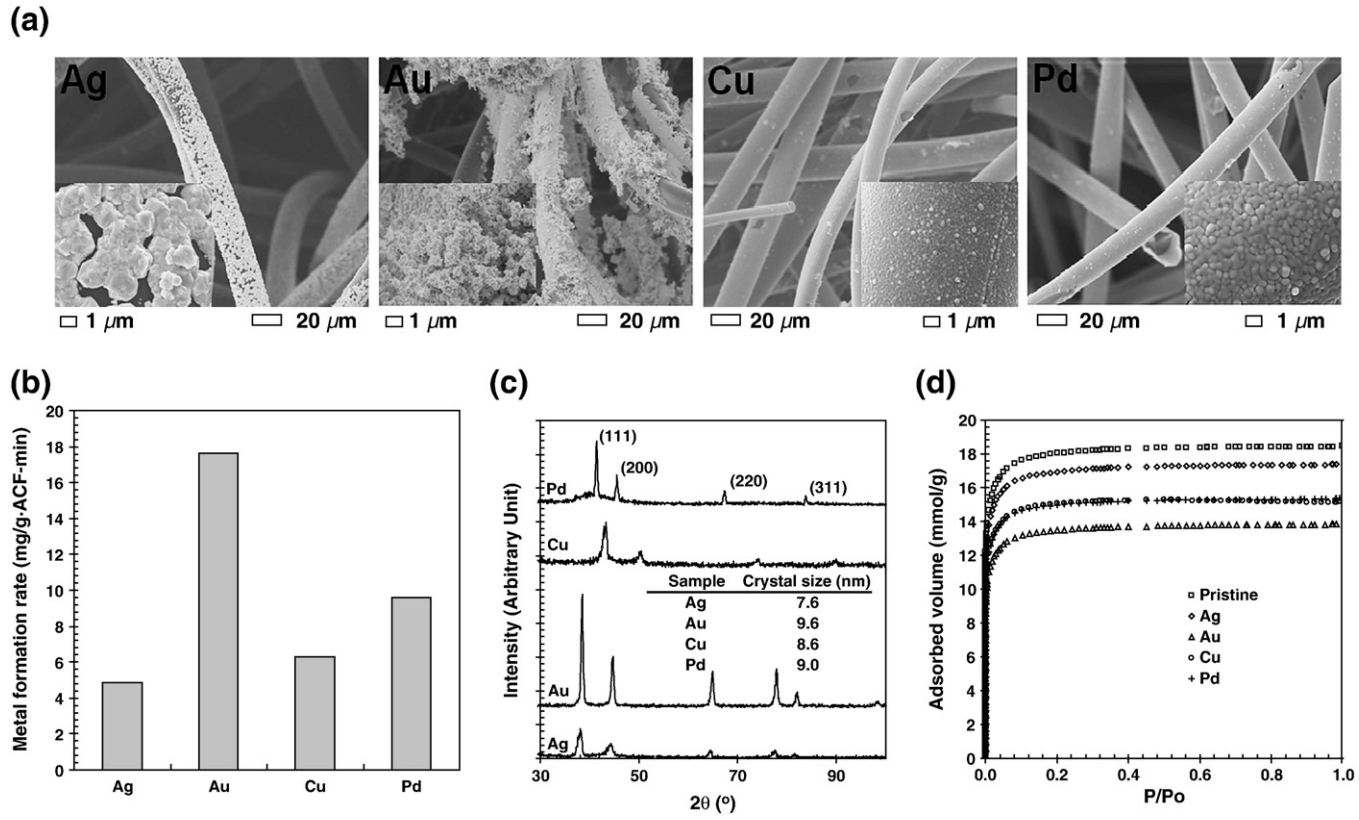

Fig. 2. Characterizations of the metal films on CF. (a) SEM micrographs. (b) Deposition rates. (c) XRD patterns with crystal sizes. (d) Nitrogen adsorption isotherms of CF with metal films.

(wet Sn–Pd activation) and did not require any wet chemical steps. A spark was generated between two identical Pd rods (diameter 3 mm, length 100 mm, Nilaco, Japan) inside a reactor under a pure nitrogen environment at standard temperature and pressure conditions. The flow rate of the nitrogen gas, which was controlled by a mass flow controller, was set to 3 L/min. The filtration was performed on both sides of the whole disc shaped CF substrate so that Pd particles could be uniformly distributed on the surfaces of the CF. The electrical circuit specifications were as follows: resistance of 0.5 MΩ, capacitance of 10 nF, loading current of 2 mA, applied voltage of 3 kV, and frequency of 667 Hz [18]. In order to prevent the detachment of nanoparticles from the CF surface, the CF substrate was separated from the holder and cured in air at 190 °C for 5 min. Once the aerosol activation was performed, the whole disc shaped CF substrate was immersed in ELD baths to be deposited with the metal and alloy films. Table 1 lists the compositions of the ELD baths and bath conditions. The CF substrate was rinsed vigorously with deionized water after ELD to remove any residual solution and then dried. Sintering of the alloy deposited CF was carried out at 400 °C in a nitrogen atmosphere for 5 h.

Field emission scanning electron microscopy (SEM, JSM-6500F, JEOL, Japan) and energy dispersive X-ray spectroscopy (EDX, JED-2300, JEOL, Japan) were performed at an accelerating voltage of 15 kV. The amount of metal elements deposited on the CF was determined by inductively coupled plasma atomic emission spectroscopy (ICPAES, Elan 6000, Perkin-Elmer, US). The X-ray diffraction (XRD) patterns of the films were obtained on a Rigaku RINT-2100 (Japan) diffractometer equipped with a thin-film attachment using Cu–$K\alpha$ radiation (40 kV, 40 mA). The nitrogen adsorption isotherms of the CF were measured using a porosimeter (ASAP 2010, Micromeritics Ins. Corp., US) at −196 °C with a pressure ratio between operation and atmosphere pressures ranging from 10^{-6} to 1. The above analysis processes were performed for a part of each CF sample.

3. Results and discussion

The first image in Fig. 1b shows low and high magnitude (inset) micrographs of the Pd aerosol activated CF. A number of particles (approximately 20 nm in diameter) were observed on the activated CF processed with an activation intensity of 0.7 mg Pd/g CF. Activation intensity (I_a) of the CF was defined as follows:

$$I_a = Qt_a m_{CF}{}^{-1} \int_0^\infty \eta(D_p) C_m dD_p \quad (1)$$

where, Q is the flow rate of nitrogen gas, t_a is the activation time, m_{CF} is the mass of the CF, $\eta(D_p)$ is the Pd nanoparticle collection efficiency of

Table 2
Atomic ratio of element in each metal film on CF after ELD.

Elemental composition (at.%)	Atomic ratio of element in metal film			
	ELD			
	Ag	Au	Cu	Pd
Pd	1.9	1.1	1.7	100.0
Au	–	98.9	–	–
Ag	98.1	–	–	–
Cu	–	–	98.3	–

Table 3
Textural properties of the CF with metal films.

Sample	Total specific surface area (m^2/g)	Micropore specific surface area (m^2/g)	Total pore volume (cm^3/g)	Micropore volume (cm^3/g)	Average pore diameter (Å)
Pristine	1624	1446	0.77	0.75	17.7
Ag	1526	1360	0.63	0.51	17.6
Au	1214	1081	0.49	0.41	16.3
Cu	1359	1211	0.60	0.46	17.0
Pd	1351	1202	0.57	0.45	16.9

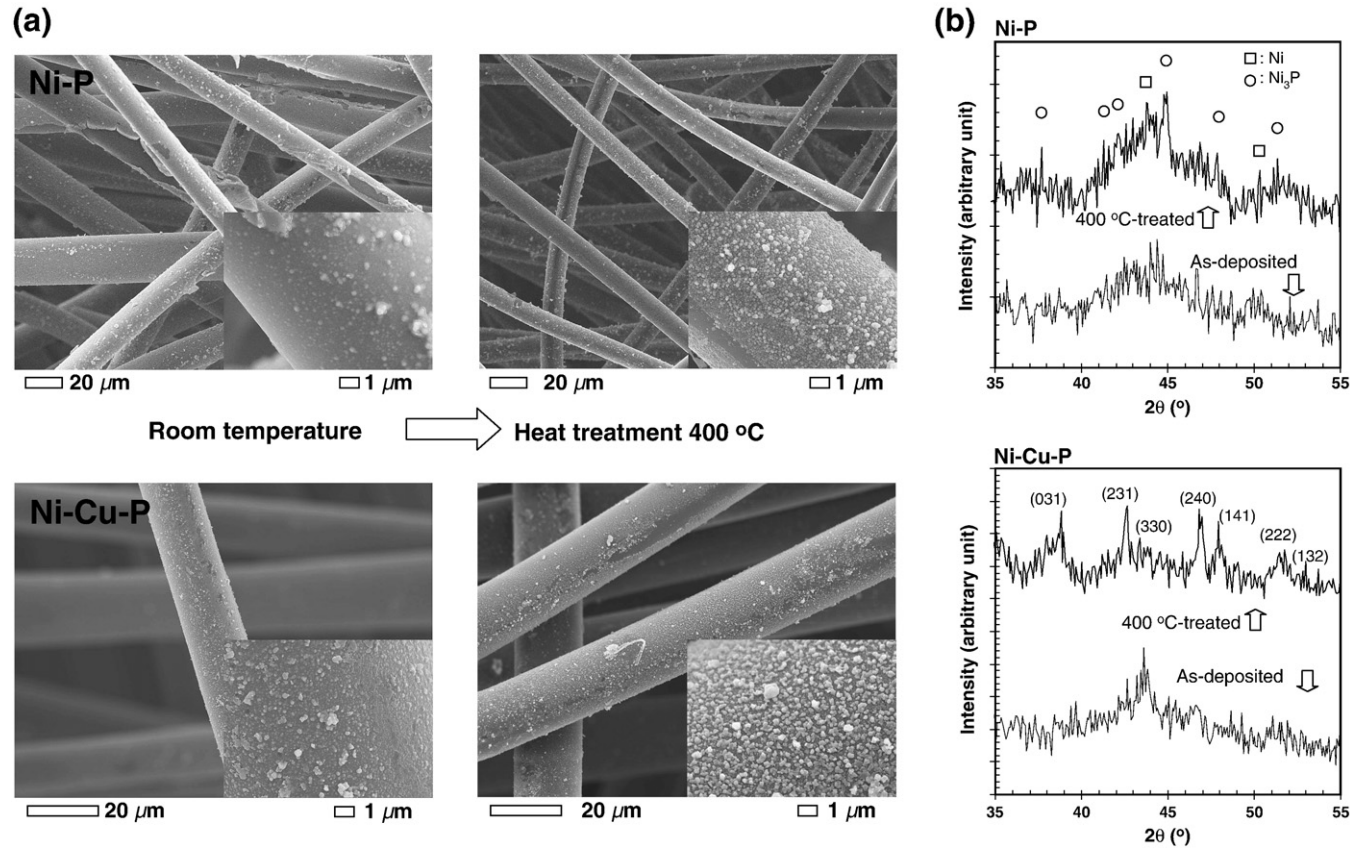

Fig. 3. SEM images (a) and XRD patterns (b) of as-deposited and sintered Ni–P and Ni–Cu–P films.

CF, and C_m (D_p) is the mass concentration of Pd nanoparticles. The following image shows an EDX map of the dotted area (inset) in the first image (for a fiber from the middle of the fabricated sample) and, the dots in the Pd K image represent the Pd particles (small white spots) distributed in the first image. From the EDX analyses (also in Fig. 1b), it was also found that activated CF contained a small amount of Pd, and the CF also contained C and O, which might have originated from the CF itself.

Fig. 2a shows low and high magnitude (inset) SEM micrographs of various metal films on the aerosol activated CF. All metal films were formed on the activated CF, even though the morphologies of each film were different. The activation intensity was uniform (0.70 mg Pd/g CF) for all the films. The films were obtained after ELD for 10 min. EDX analyses (not shown) revealed that the metal films consisted mainly of pure Ag, Au, Cu, or Pd. However, they contained a small amount of Pd. From the elemental data (Table 2), the deposited metal species originated from the metal ions in the ELD bath. The deposition amounts of the metal films were calculated by ICPAES analyses. Analysis for film was performed as follows. A weighed portion of the sample (about 0.1 g) was dissolved in 5 mL of boiling HNO_3. The resulting solution was diluted with water to 50 mL in a volumetric flask. The corresponding deposition rates for Ag, Au, Cu, and Pd were 4.86, 17.61, 6.30, and 9.57 mg metal/g CF min, respectively (Fig. 2b). The differences in deposition rates were caused by different growth kinetics of Ag, Au, Cu, and Pd ELD, even though all the films were deposited at the same activation intensity. XRD results (Fig. 2c) show peaks corresponding to the (111), (200), (220), and (311) planes of the face-centered cubic (fcc) phases of the corresponding metals, as referenced to joint committee on powder diffraction standard (JCPDS) files. The average crystal sizes estimated from the XRD line broadening of the (111) peak, according to Scherrer's equation ($t = 0.9\lambda/(B\cos\theta)$), were 7.6, 9.6, 8.6 and 9.0 nm for the Ag, Au, Cu, and Pd films, respectively. The different intensities of the metal peaks also revealed different growth kinetics (shown in Fig. 2b) between films. Fig. 2d shows that major uptake of nitrogen adsorption occurred at a relatively low pressure ($P/P_o < 1$) reaching a plateau at $P/P_o \approx 0.3$ for a part of the whole disc shaped sample. This suggests that all the CF had microporous characteristics (type I isotherm) according to the international union of pure and applied chemistry classification [27]. The adsorbed volume was the largest for the pristine CF and decreased for the CF with the metal films because the films can obstruct or reside in some of the pores in the pristine CF. Table 3 summarizes the textural properties of the samples. The largest decrease in porosity was detected for Au, which was attributed to its highest deposition rate. Table 3 also shows that the pore size distribution of the samples was concentrated at pore diameters <20 Å (i.e. microporous).

Table 4
Atomic ratio of element in each alloy film on CF after ELD.

Elemental composition (at.%)	Atomic ratio of element in alloy film	
	ELD	
	Ni–P	Ni–Cu–P
Pd	1.6	0.6
Ni	87.6	73.4
P	10.8	13.6
Cu	–	12.4

Fig. 3a shows low and high magnification (inset) SEM micrographs of Ni–P and Ni–Cu–P electroless films on the activated CF. Particles were deposited from both the Ni–P and Ni–Cu–P baths. Therefore, Pd aerosol activation can be used effectively in alloy ELD processes. Fig. 3a also shows the results for the 400 °C-treated Ni–P and Ni–Cu–P films. The corresponding crystallization behaviors of the as-deposited and 400 °C-treated Ni–P and Ni–Cu–P films were examined by XRD (Fig. 3b). There was a slight difference in the diffraction patterns between the as-deposited and 400 °C-treated Ni–P films. The diffuse diffraction peak of the as-deposited Ni–P film indicates an amorphous

microstructure. However, some sharp peaks were observed for the 400 ºC-treated Ni–P, which were caused mainly by a transformation of amorphous phases to Ni and Ni_3P [28]. Fig. 3b also shows the XRD patterns of the as-deposited and 400 °C-treated Ni–Cu–P films. The as-deposited films were mainly amorphous, similar to the as-deposited Ni–P. On the other hand, the films sintered at 400 °C showed tetragonal Ni_3P [22]. This suggests that Ni_3P crystallization was promoted during sintering by the presented Cu. The increased crystallinity in the film might be due to the addition of Cu to a Ni–P deposit, which increased the relative P/Ni ratio (described in Table 4) [29]. The deposition amounts (Ni and Cu) of the alloy films were calculated by ICPAES analyses. The P content was determined photocolorimetrically by the standard procedure [30].

Electrical resistivity of the alloy deposited samples with both before and after heat treatment was briefly checked. Four probe tips were connected to a part of the sample (the downward force of approximately 0.1 kg per probe), then the electrical resistance (R) was determined by measuring the voltage–current data (at 22 °C temperature and 54% relative humidity) across the sample. The resistivity (ρ) was calculated using the following relationship:

$$\rho = \frac{RA}{L} \tag{2}$$

where A and L are the cross-sectional area and length of the sample, respectively. The resistivities before the heat treatment of as-deposited Ni–P and Ni–Cu–P were from 336 to 264 μΩ cm, respectively. After the heat treatment, there is an increase in the number of crystalline phases (or more conductive paths) on the films, resulting in a decrease in resistivity (238 μΩ cm for Ni–P and 91 μΩ cm for Ni–Cu–P).

4. Summary

Pd aerosol activation on CF can initiate the growth of metal and alloy films. This method of activation can be used widely for depositing a variety of electroless films. Sintering the alloy films with different elemental composition resulted in crystallization behavior. This aerosol assisted process can be used to produce various metallic film/substrate configurations being used in various fields of materials technology such as environmental catalysts, reinforced materials, antimicrobial agents, electromagnetic interference shielding materials, and electrolysis cells.

Acknowledgement

The authors wish to thank to the Korea Energy Management Corporation (KEMCO) through Grant No. 2008-N-PV08-P-06-0-000 for supporting this research.

References

[1] J.H. Byeon, H.S. Yoon, K.Y. Yoon, S.K. Ryu, J. Hwang, Surf. Coat. Technol. 202 (2008) 3571.
[2] J. Jang, S.K. Ryu, J. Mater. Process. Technol. 180 (2006) 66.
[3] J.H. Byeon, K.Y. Yoon, J.H. Park, J. Hwang, Carbon 45 (2007) 2313.
[4] K.Y. Yoon, J.H. Byeon, C.W. Park, J. Hwang, Environ. Sci. Technol. 42 (2008) 1251.
[5] S.-S. Tzeng, F.-Y. Chang, Thin Solid Films 388 (2001) 143.
[6] E. Neubauer, G. Korb, C. Eisenmenger-Sittner, H. Bangert, S. Chotikaprakhan, D. Dietzel, A.M. Mansanares, B.K. Bein, Thin Solid Films 433 (2003) 160.
[7] Y. Fan, H. Yang, X. Liu, H. Zhu, G. Zou, J. Alloys Compd. 461 (2008) 490.
[8] S.-S. Tzeng, Carbon 44 (2006) 1986.
[9] X. Changrong, G. Xiaoxia, L. Fanqing, P. Dingkun, M. Guangyao, Colloids Surf. A: Physicochem. Eng. Aspects 179 (2001) 229.
[10] X. Gan, Y. Wu, L. Liu, B. Shen, W. Hu, J. Alloys Compd. 455 (2008) 308.
[11] J. Gao, F. Tang, J. Ren, Surf. Coat. Technol. 200 (2005) 2249.
[12] E. Gasana, P. Westbroek, J. Hakuzimana, K.D. Clerck, G. Priniotakis, P. Kiekens, D. Tseles, Surf. Coat. Technol. 201 (2006) 3547.
[13] H. Jha, T. Kikuchi, M. Sakairi, H. Takahashi, Mater. Lett. 63 (2009) 1451.
[14] J.-Y. Lee, S. Horiuchi, Thin Solid Films 515 (2007) 7798.
[15] Y. Kobayashi, Y. Tadaki, D. Nagao, M. Konno, J. Colloid Interface Sci. 283 (2005) 601.
[16] Y.-J. Oh, S.M. Cho, C.-H. Chung, Electrochem. Solid-State Lett. 8 (2005) C1.
[17] J.H. Byeon, J.H. Park, J. Hwang, J. Aerosol Sci. 39 (2008) 888.
[18] J.H. Byeon, B.J. Ko, J. Hwang, J. Phys. Chem. C 112 (2008) 3627.
[19] H. Ma, F. Tian, D. Li, Q. Guo, J. Alloys Compd. 474 (2009) 264.
[20] T. Saeid, S. Yazdani, N. Parvini-Ahmadi, Surf. Coat. Technol. 200 (2006) 5789.
[21] S. Armyanov, J. Georgieva, D. Tachev, E. Valova, N. Nyagolova, S. Mehta, D. Leibman, A. Ruffini, Electrochem. Solid-State Lett. 2 (1999) 323.
[22] M. Murayama, A. Belyakov, T. Hara, Y. Sakai, K. Tsuzaki, M. Okubo, E. Eto, T. Kimura, J. Electron. Mater. 35 (2006) 1787.
[23] G. Stremsdoerfer, H. Omidvar, P. Roux, Y. Meas, R. Ortega-Borges, J. Alloys Compd. 466 (2008) 391.
[24] K. Ziewiec, J. Alloys Compd. 397 (2005) 207.
[25] A.A. Baker, C. Shipman, P.W. Jackson, Fibre Sci. Technol. 5 (1972) 213.
[26] S.J. Baker, W. Bonfield, J. Mater. Sci. 13 (1978) 1329.
[27] S. Brunauer, P.H. Emmett, E. Teller, J. Am. Chem. Soc. 60 (1938) 309.
[28] R. Touir, H. Larhzil, M. Ebntouhami, M. Cherkaoui, E. Chassaing, J. Appl. Electrochem. 36 (2006) 69.
[29] H. Ashassi-Sorkhabi, H. Dolati, N. Parvini-Ahmadi, J. Manzoori, Appl. Surf. Sci. 185 (2002) 155.
[30] L.B. Belykh, N.I. Skripov, L.N. Belonogova, V.A. Umanets, F.K. Shmidt, Russ. J. Appl. Chem. 80 (2007) 1523.